

# **The non-resonant kink modes triggering strong sawtooth-like crashes in the EAST tokamak**

Erzhong Li<sup>1</sup>, V. Igochine<sup>2</sup>, O. Dumbrajs<sup>3</sup>, L. Xu<sup>1</sup>, K. Chen<sup>1</sup>, T. Shi<sup>1</sup>,  
and L. Hu<sup>1</sup>

1 Institute of Plasma Physics, Chinese Academy of Science, Hefei  
230031, People's Republic of China

2 MPI fur Plasmaphysik, D-85748 Garching, Germany

3 Institute of Solid State Physics, Kengaraga Street 8, LV-1063, Riga,  
Latvia

E-mail: [rzhonglee@ipp.ac.cn](mailto:rzhonglee@ipp.ac.cn), [lqhu@ipp.ac.cn](mailto:lqhu@ipp.ac.cn)

## **Abstract**

Evolution of the safety factor ( $q$ ) profile during L-H transitions in Experimental Advanced Superconducting Tokamak (EAST) was accompanied by strong core crashes before regular sawtooth behavior. These crashes appeared in the absence of  $q=1$  ( $q$  is the safety factor) rational surface inside the plasma. Analysis indicates that the  $m/n=2/1$  tearing mode is destabilized and phase-locked with the  $m/n=1/1$  non-resonant kink mode (the  $q=1$  rational surface is absent) due to the self-consistent evolution of plasma profiles as the L-H transition occurs ( $m$  and  $n$  are the poloidal and toroidal mode numbers, respectively). The growing  $m/n=1/1$  mode destabilizes the  $m/n=2/2$  kink mode which eventually triggers the strong crash due to an anomalous heat conductivity,

as predicted by the transport model of stochastic magnetic fields using experimental parameters. It is also shown that the magnetic topology changes with the amplitude of  $m/n=2/2$  mode and the value of center safety factor in a reasonable range.

## **1 Introduction**

The macroscopic magnetohydrodynamics (MHD) instabilities in core are important for the global confinement of fusion plasmas in tokamaks [1]. The well-known instability is the sawtooth crash which periodically limits the core pressure [2-3], triggers kinds of MHD instabilities such as the neoclassical tearing mode (NTM) [4-5], and redistributes energetic particles or impurities etc [6-8]. The sawtooth crashes were regarded as self-consistent evolutions of the plasma current density, pressure or/and safety factor ( $q$ ) profiles, periodically modifying the stability boundary of internal kink mode around the  $q=1$  rational surface [9-11]. Depending on characteristics of sawtooth crashes, two different mechanisms, such as the magnetic reconnection and quasi-interchange models, have been proposed in last years [12-13]. It was generally assumed that the nonlinear development of  $m/n=1/1$  kink mode ( $m, n$  are the poloidal and toroidal mode number, respectively) eventually triggered sawtooth crashes [14-15]. In experiments, the active control has successively suppressed sawtooth oscillations by means of heating or current driving [16-20].

In recent years, it was reported a so-called long-lived mode (LLM) of

$m/n=1/1$  which was saturated and did not trigger sawtooth oscillations in MAST [21]. The stability analysis indicated that it was an ideal kink mode with a flat  $q$  profile in core, a  $q$ -value near or above unity (i.e., weak or reversed magnetic shear) [22]. The above characteristic of  $q$ -profile probably leads to a non-resonant kink mode, meaning the mode is not localized at the  $q=1$  rational surface [22-25]. As far as the  $q$ -profile relaxes, this long-lived mode resulted in normal sawtooth crashes and standard sawtooth behaviors at the later phase of the discharges. In addition, there were also experimental observations of snake-like kink oscillations, in the cases with and/or without sawteeth [26-31]. Up to present, two explanations were available: the bifurcation of tokamak equilibrium states and the nonlinear MHD evolution assuming the density separation from plasma pressure [32-33]. However, there are still many aspects contradicting each other [34-36].

The kink modes mentioned above may have different destabilizing mechanisms, but the resulting perturbations locate in core either referring to sawtooth crashes or to long-lived oscillations, or to a seed island triggering NTM. The present experiment shows a similar structure of  $m/n=1/1$  kink mode, but it is coupled with the  $m/n=2/1$  tearing mode. In particular, it leads to strong sawtooth-like crashes (or big crashes) in the core. In what follows we describe a detailed observation of behavior of perturbations in Section 2, then discuss the existed models for crashes in

Section 3 and demonstrate a candidate explanation in Section 4, and arrange the conclusion in Section 5.

## 2 Observation

MHD perturbations in EAST ( $R_0 \approx 180\text{ cm}$ ,  $a \approx 50\text{ cm}$ ) show a series of novel characteristics. As illustrated in Figure 1 (a typical shot: 34484), MHD oscillations start just after the L-H transition indicated by D-alpha radiation in (a) which can be observed in soft x-ray (SX) radiation (a) and Mirnov signals (b) almost simultaneously. Particularly, there are two sawtooth-like crashes (denoted by 'big crashes') in (a) which are accompanied by the increasing amplitude of magnetic oscillations as indicated by the curves in (b). The relative intensity of SX does not regain from the big crashes in contrast to the regular sawtooth crashes (ST). In this way, they are similar to the well-known minor disruptions but occurring only in the plasma core. On the other hand, big crashes are always accompanied by MHD oscillations. This is also different from sawtooth cycles with precursor and/or post-cursor oscillations. Empirically it is difficult to detect the MHD oscillations of sawtooth cycles with Mirnov coils because the sensor coils are too far from the  $q=1$  rational surface in EAST. However, there are significant magnetic perturbations of Mirnov sensors in figure 1(b). Analysis of spatially distributed magnetic sensors indicates that the mode mainly has the  $m/n=2/1$  helical structure.

The evolutions of MHD modes in SX signals during the first two big crashes are illustrated in figure 2(a) and figure 2(b), respectively. Perturbations exist across a broad space from  $Z=-2.73\text{cm}$  to  $Z=-20.52\text{cm}$ , and big crashes occur without the inversion radius as indicated by the two vertical arrows. This is in contrast to the subsequent regular sawtooth crashes in figure 2(c) where the inverse sawtooth appears gradually inwards as indicated by the vertical arrows. The inversion radius is also expected to evolve in the same way. In addition, the superimposed MHD oscillations disappear first within  $Z=-7.8\text{cm}$ . Figure 3 shows the SX profiles round ST crashes (before: circle; after: plus) at several time moments as indicated by the arrows in figure 2(c). Clearly, the inversion radius changes from  $Z=-18\text{cm}$  to about  $Z=-13\text{cm}$ . The evolution of inversion radius indicates the relaxation of current profile. Initial central  $q$  is larger than unity but becomes smaller at later stage. At this time, the first normal sawtooth appears in the plasma. This is a natural result of changes in plasma profiles due to the transition to H-mode. It should be emphasized that the absence of inversion radius for the big crashes corresponds to the center  $q$  larger than unity.

The main features of MHD perturbations in the big crash (we choose the first one) are illustrated in figure 4. The available SX measurements in the outer and core chords are shown in figure 4(a) and figure 4(b), respectively. Significant MHD oscillations begin just at the L-H transition

(indicated by the decreasing D-alpha radiation), and seriously modify the core SX profile as illustrated in the contour plot in figure 4(c). The start point basically coincides with the magnetic perturbations, as illustrated by the time frequency spectrum of Mirnov signals in figure 4(d). However, perturbations seem to be lagging a little behind the L-H transition, indicating that the driving source comes from the L-H transition, by the change of profile such as the current density. It can be further inferred that the measured  $m/n=2/1$  mode is probably the tearing mode. The figure 4(e) shows the perturbation magnetic flux. However, it is unnecessary to distinguish the tearing mode from the kink mode for the  $m/n=2/1$  perturbations, while the perturbation on SX signals belongs to kink modes with  $m/n=1/1$  and  $m/n=2/2$  helical structures. This will be discussed in what follows.

The mode coupling between  $m/n=2/1$  and  $m/n=1/1$  is clearly seen in figure 5. The  $m/n=2/1$  mode in figure 5(c) is destabilized nearly at the moment when the  $m/n=1/1$  mode gets measured at  $Z = 12\text{ cm}$  in figure 5(b). However, the perturbation amplitude is obviously larger at  $Z = 12\text{ cm}$  than at  $Z = 0.23\text{ cm}$  in figure 5(a). In addition, the  $m/n=1/1$  mode has the same frequency as the  $m/n=2/1$  mode. This is a strong evidence for the  $m/n=1/1$  mode coupling with the  $m/n=2/1$  mode. The phase-locked modes grow and destabilize the  $m/n=2/2$  mode in figure 5(a) and 5(b). As a consequence of mode growth, the big crash is eventually

triggered as indicated by the vertical line.

The spatial structures of kink modes are identified in figure 6 which are calculated by means of the fast Fourier transformation (FFT) over the time before the big crash. It is obvious that the profiles for  $m/n=1/1$  are basically axisymmetric around the magnetic axis indicated by the vertical line (We used the absolute value of amplitude in plotting to avoid asymmetry). The magnetic axis drifts a bit downward because of the down single-none (DSN) equilibrium configuration. The appreciable perturbation is within about 6cm away from the magnetic axis, corresponding to  $r/a \approx 0.12$ . However, the  $m/n=2/2$  mode has a bigger width about  $r/a \approx 0.22$ . Evolutions of both modes are illustrated in figure 7 where the vertical line indicates the big crash. Only with the FFT amplitudes, this is clearly due to the fast growth of  $m/n=2/2$  mode in figure 7(a) in comparison to the  $m/n=1/1$  mode in figure 7(c). However, once including the oscillating phase, it gets difficult to determine which mode eventually leads to the big crash as shown in figures 7(b) and 7(d).

### **3 Discussion**

It is analyzed as above that the dynamics of  $m/n=2/2$  mode plays an important role for this category of strong crash. The whole evolution demonstrates that the  $q=1$  rational surface is absent in plasma during the strong crashes. This means that the modes of  $m/n=1/1$  and  $m/n=2/2$  are classified as non-resonant modes. Both modes can deform the magnetic

surface without reconnection as shown in figure 4(c). The distortion of magnetic surfaces gradually gets stronger because of the  $m/n=1/1$  mode phase-locked with the  $m/n=2/1$  tearing mode. In particular, the destabilized  $m/n=2/2$  mode exhibits a twice frequency of the  $m/n=1/1$  mode, implying a secondary distortion of the perturbed magnetic surface. There are possible other high-order modes in braiding magnetic field lines, but they may be too microscopic to be detected due to the present spatial resolution of diagnostics. In addition, there is no measurable magnetic reconnection event for formation of magnetic island in the contour plot of SX signals. This states that the reconnection model which generally occurs at the  $q=1$  rational surface can not explain this strong crash. However, there is another model called the quasi-interchange model in explaining sawtooth crash. A broad region with  $q \approx 1$  ( $q$  is the safety factor) in the core is necessary, and the hot crescent core and cold bubble shall be characterized. Although the required time scale ( $\sim 100 \mu s$  much closer to the ideal MHD time scale rather than the resistive one) for the crash is in the same magnitude as that observed in this experiment, the growth of the  $m/n=2/2$  mode can not be predicted by this model and the main feature of a pair of hot-crescent and cold-bubble was also not measured.

Actually, the relevance of strong crash with the increasing magnetic perturbations indicates the dependence of heat transport coefficient



(thermal conductivity) on the change of magnetic topology. The strong crash shall be the result of promptly enhanced anomalous heat conductivity due to the presence of higher-n ( $n > 1$ ) modes which braid the magnetic field lines. Significant progress in theory and experiments were made on the onset of crash induced by braiding magnetic field lines [37-38]. One theory indicated that the thermal conductivity can be enhanced by a factor  $\sim \sqrt{m_i/m_e}$  in the stochastic (braiding) magnetic topology in comparison to the electrostatic limit [37]. The criterion for triggering the stochasticity of magnetic field lines requires that a dimensionless parameter of pressure gradient is bigger than the magnetic shear. This model seems to agree with observations just after the L-H transition and before the first strong crash, such as the increasing pressure reflected by the ramping-up SX radiation in figure 1(a) and the weak or even a little negative magnetic shear indicated by the absence of  $q=1$  rational surface. However, it is again difficult to explain the necessity of the presence of  $n=2$  ( $m/n=2/2$ ) mode for the strong crash in experiments.

The other theory investigated the self-consistent change of parallel current density and the perturbed magnetic field [39]. The thermal conductivity in strong stochastic case is proportional to the product of electron thermal velocity and the square of perturbed magnetic field ( $\chi_e \sim V_{te}(\tilde{b}/B)^2 L_c$ ,  $L_c$  is the correlation length of stochasticity), which is large enough to predict the crash. The modification of current density

profile either distorts the magnetic surface or destabilizes other modes, which depends on the sign of the secondary derivative of perturbed current. The generation of higher- $n$  mode is as a result of increasing the magnetic energy to balance the destabilizing free energy, and braiding magnetic field lines with a spectrum of different  $n$ -mode leads to a stochastic region. This can explain why the  $m/n=2/2$  mode is destabilized just before the crash. In present experiments the low hybrid wave (LHW) is the unique auxiliary heating and current-driving method which is largely in support of this explanation.

It should be noted that the phase-locked  $m/n=1/1$  and  $m/n=2/1$  modes are driven by the change of equilibrium profiles (current and/or pressure) when the plasma enters into the H-mode phase. The magnetic perturbations induced by the  $m/n=2/1$  mode easily penetrate inwards and interact with the  $m/n=1/1$  non-resonant kink mode since the  $q=1$  rational surface (as the current shielding layer) is absent in plasma. This effectively increases the amplitude of  $m/n=1/1$  mode which can further disturb parallel current density. The latter can destabilize the  $m/n=2/2$  mode in terms of the suggested model in Ref.[39]. Of course, one can also not exclude the contribution of plasma pressure in destabilizing the modes and resulting in the stochastic region.

#### **4 Candidate explanation**

The absence of a reliable  $q$ -profile makes us explain the above

observations in a qualitative way. In this section, we only want to demonstrate how the  $m/n=2/2$  mode changes the magnetic topology. Based on the value of  $q_{95} = 3.3$  and an assumption of  $q_0 = 1.01$  as the  $q=1$  rational surface is absent in plasmas, we can fit a  $q$ -profile by the second order polynomial as shown in figure 8(a). The perturbed fluxes for observed modes are parametrically plotted in figure 8(b) where ratio of the core amplitude for the  $m/n=2/1$  mode is chosen as seven times of the measured perturbed flux at edge. The  $m/n=1/1$  mode amplitude is smaller than the  $m/n=2/1$  core amplitude with a factor of  $\varepsilon = a/R_0$ , and the ratio of the relative amplitude of  $m/n=2/2$  mode to that of the  $m/n=1/1$  mode is two as the measured value. Actually, it is still challenging to get the exact perturbed fluxes in experimental study. With this input, we can use the mapping technique of Hamiltonian problem to investigate the topology of magnetic fields. This method has been successfully applied in ASDEX Upgrade [40-41], HT-7 [42] etc, which will not be elaborated here.

The Poincare plots as outputs are shown in figure 9 where the upper one (figure 9(a)) was calculated with the perturbed fluxes of  $m/n=2/1$  mode and  $m/n=1/1$  mode. The rational surface of  $m/n=2/1$ , according to figure 8(b), is at about  $r/a = 0.65$  which is far away from the considering core region  $r/a < 0.22$ . It is obvious that the  $m/n=2/1$  mode has a robust perturbation forcing the field line to bend a bit in the core. However, inclusion of the  $m/n=2/2$  perturbation flux leads to a significant change of

the topology. As is shown in figure 9(b), there are a lot of belt-like stochastic zones within  $r/a < 0.14$ . In particular, there is an island-like braiding which connects the inside stochastic region to the outside nested surfaces, as indicated by the arrow. According to the EFIT equilibrium calculation, this scope corresponds to a spatial scale within about  $Z < 8\text{cm}$  where strong sawtooth-crashes were observed in experiments. To illustrate the dependence of stochasticity on the  $m/n=2/2$  mode, we sweep its amplitude around the value ( $A_{2,2}$ ) in figure 8(b) and keep other parameters invariant. The result is shown in figure 10 where we show four different amplitudes of  $m/n=2/2$  mode such as  $0.1A_{2,2}$  in figure 10(a),  $0.5A_{2,2}$  in figure 10(b),  $0.75A_{2,2}$  in figure 10(c) and  $1.25A_{2,2}$  in figure 10(d). It is clear that the stochastic belt is extended with increase of the amplitude of  $m/n=2/2$  mode, as illustrated from figure 10(a) to figure 10(c). In particular, as the amplitude is closer to and bigger than the  $A_{2,2}$ , a new braiding structure is formed around  $r/a \approx 0.12$  which is similar to an island of  $m/n=2/2$  ( $\Delta W_n$  labels the width) in figure 10(d). It is illustrated that the formation of x-point can be ascribed to the increasing amplitude of  $m/n=2/2$  mode. As a result, it short-circuits the inside stochastic and the outside nested surfaces in figure 10(d).

With these identifications, we can further check the heat conductivity which was derived as follows [39]:

$$\chi_e = 5 \times 10^{-2} \frac{V_{te} R}{q^3 s^2} \left(\frac{r}{R}\right)^2 \left(\frac{\alpha}{N}\right)^2 \quad (1)$$

Where  $q$  is the safety factor and  $s$  is the local magnetic shear.  $\alpha \geq 1$  is the parameter reflecting the degree of stochasticity and  $N$  is the maximum of the toroidal mode number (We assume  $N=2$  since the other higher  $n$  mode is not measured in experiments). The electron thermal velocity is  $V_{te} = 5.9 \times 10^5 \sqrt{T_e [eV]} \approx 2.3 \times 10^7 \text{ m/s}$  ( $T_e \approx 1.5 \text{ keV}$ ). The magnetic shear is  $s \leq 0.1$  round the location ( $r/a \approx 0.12$ ) of the braiding structure. With these parameters, it is then derived that the value of thermal conductivity is at least  $\chi_e \geq 0.05 \text{ m}^2 / \mu\text{s}$ . We therefore can estimate the duration of the strong crash which is assessed as  $\tau = 2\pi Ra / \chi_e \approx 113 \mu\text{s}$  by assuming that the core energy is fully conducted to edge. It should be indicated that this estimation probably overestimate the real duration of crash a little higher since the real thermal conductivity may be much larger. However, this is in agreement with the observed value of  $\sim 100 \mu\text{s}$ , at least in the same order of magnitude.

It is important to note that in the present case the tearing mode ( $m/n=2/1$ ) has its rational surface inside the plasma and there is no rational surface inside plasma for non-resonant kink modes ( $m/n=1/1$  and  $m/n=2/2$ ). This situation is different from the standard sawtooth crash where the  $q=1$  rational surface is always inside the plasma. To demonstrate the dependence of the magnetic topology on the center safety factor  $q_0$ , we show several snapshots in figure 11 where the figure 11(a) is the repeat of figure 9(b). It is observed that the braiding takes shape in

figure 11(a), exhibits the  $m/n=2/2$  island structure which is isolated from the stochastic region as the center safety factor decreases in figure 11(b), and becomes a clear island with the stochastic regions further shrinking at  $q_0 = 0.97$  in figure 11(c). Further more, stochastic regions fully disappear when the  $m/n=2/2$  mode is absent as seen in figure 11(d). This again illustrates the significance of  $m/n=2/2$  mode for the strong crash. At last, it should be indicated that scanning the shape of  $m/n=2/1$  mode in a reasonable range does not change the above results.

## 5 Conclusion

The  $m/n=2/1$  tearing mode was destabilized and phase-locked with the  $m/n=1/1$  non-resonant kink mode (the center safety factor is larger than unity) during the L-H transitions, and the strong crash occurred with further growth of  $m/n=2/2$  mode. Above a critical amplitude of  $m/n=2/2$  mode, the magnetic field lines were converted into significant stochastic region which was short-circuited with the outside nested surfaces by a braiding of  $m/n=2/2$  mode. Experimental observation of the duration of strong crash ( $\sim 100\mu s$ ) agreed with the prediction using the stochastic transport model.

The strong core crash induced by non-resonant kink modes of  $m/n=1/1$  and  $m/n=2/2$  requires the center safety factor  $q_0$  a little bigger than one, which actually does not occur again after regular sawtooth crashes reappearing. It is inferred that the future discharge with a flat

q-profile (weak magnetic shear) in the absence of  $q_0 = 1$  surface in plasmas may suffer from the similar limit. This may be encountered in H-mode experiments for advanced operation scenarios, needing to be carefully controlled by optimization of the current density profile. However, this study is still initial, and we hope to use the MSE-confined (Motional Stark Effect) equilibrium reconstruction and high-resolution diagnostics (such as electron cyclotron emission (ECE)) to investigate the strong core crashes on EAST in future.

### **Acknowledgement**

This work is supported by the National Natural Science Foundation of China under Grant No. 11405216 and the JSPS-NRF-NSFC A3 Foresight Program in the field of Plasma Physics (NSFC No.11261140328).

### **Reference**

- [1] Hender T C et al 2007 Nucl. Fusion 47 S128
- [2] von Goeler S et al 1974 Phys. Rev. Lett. 33 1201
- [3] Wesson J A et al 1986 Plasma Phys. Control. Fusion 28 243
- [4] Chapman I T et al 2011 Plasma Phys. Control. Fusion 53 013001
- [5] Sauter O et al 2002 Phys. Rev. Lett. 88 105001
- [6] Kolesnichenko Ya I et al 1996 Nucl. Fusion 36 159
- [7] Maraschek M et al 2005 Nucl. Fusion 45 1369
- [8] Nave M F F et al 2003 Nucl. Fusion 43 1204
- [9] Park W et al 1991 Phys. Fluids B 3 507

- [10] Bateman G et al 2006 Phys. Plasmas 13 072505
- [11] Porcelli F et al 1996 Plasma Phys. Control. Fusion 38 2163
- [12] Kadomtsev B B et al 1975 Sov. J. Plasma Phys. 1 389
- [13] Wesson J A 1986 in Plasma Phys. Control. Fusion (Proc. 12th European Conf, Budapest, 1985) 28, 1A, 243
- [14] Hastie R J et al 1988 Nucl. Fusion 28 585
- [15] Bussac M N et al 1975 Phys. Rev. Lett. 35 1638
- [16] Furno I et al 2001 Nucl. Fusion 41 403
- [17] Graves J P et al 2009 Phys. Rev. Lett. 102 065005
- [18] Graves J P et al 2003 Phys. Plasmas 10 1034
- [19] Chapman I T et al 2007 Phys. Plasmas 14 070703
- [20] Chapman I T et al 2006 Nucl. Fusion 48 035004
- [21] Hua M D et al 2010 Europhys. Lett. 90 55001
- [22] Chapman I T et al 2010 Nucl. Fusion 50 045007
- [23] Wahlberg C et al 2007 Phys. Plasmas 14 110703
- [24] Hastie R J et al 1987 Phys. Fluids 30 1756
- [25] Guo S C et al 2013 Nucl. Fusion 53 113035
- [26] Breslau J A et al 2011 Nucl. Fusion 51 063027
- [27] Wang F et al 2013 Phys. Plasmas 20 072506
- [28] Shi T et al 2013 Plasma Phys. Control. Fusion 55 055007
- [29] Xu L et al 2012 Phys. Plasmas 19 122504
- [30] Delgado-Aparicio L et al 2013 Phys. Rev. Lett. 110 065006



- [31] Gill R D et al 1992 Nucl. Fusion 32 723
- [32] Cooper W A et al 2011 Plasma Phys. Control. Fusion 53 124005
- [33] Sugiyama L E 2013 Phys. Plasmas 20 032504
- [34] Delgado-Aparicio L et al 2013 Nucl. Fusion 53 043019
- [35] Wesson J A 1995 Plasma Phys. Control. Fusion 37 A337
- [36] Cooper W A et al 2011 Nucl. Fusion 51 072002
- [37] Itoh K et al 1995 Plasma Phys. Control. Fusion 37 707
- [38] Itoh S-I et al 1998 Plasma Phys. Control. Fusion 40 879
- [39] White R et al 1989 Phys. Fluids B 1 977
- [40] Igochine V et al 2007 Nucl. Fusion 47 23
- [41] Dumbrajs O et al 2005 Phys. Plasmas 12 110704
- [42] Li E et al 2011 Plasma Phys. Control. Fusion 53 085019

### **Figure captions**

Figure 1. The characteristic of core MHD perturbation for the typical shot 34484: (a) the soft x-ray (SX) radiation in the centre chord (up trace) and the D-alpha ray used to indicate the L-H transition (down trace), and (b) the Mirnov oscillations. MHD perturbations are simultaneously excited just after the L-H transition (dash line) on both SX and Mirnov signals. Two strong sawtooth-like crashes denoted by 'big crash' in (a) are obviously different from the following regular sawtooth crashes (ST) as indicated by vertical arrows. The vertical dash line labels the L-H transition when MHD oscillations are excited.

Figure 2. The evolution of SX signals across major interested region at several time slices: (a) during the first big crash, (b) during the second big crash, and (c) with regular sawtooth crashes. One can not find the inversion radius in (a) and (b) while this can be observed in (c). In addition, the inversion radius shrinks with time in (c) indicating the change of  $q=1$  rational surface. However, the  $q=1$  rational surface is absent for the big crashes.

Figure 3. The profiles of SX radiation in the figure 2(c): data from the averaging relative intensity round the first arrow, during the time window round the second and third arrows, as well as the fifth and sixth arrows from upper to down panels, respectively. The change of inversion can be clearly seen.

Figure 4. The time window for the analysis of the big crash: (a) the available SX signals in the most outside chords ( $Z \approx \pm 12\text{cm}$ ), (b) the core SX signals at  $Z = 0.23\text{cm}$  as well as the D-alpha radiation, (c) contour plot of SX signals in interested region, (d) time frequency spectrum of Mirnov signals with the raw signals superimposed and (e) the resulting perturbation magnetic flux at edge. The arrows across (b) and (c) indicate the strengthening perturbations in core, while the vertical line labels the moment of the big crash.

Figure 5. The evolutions of the frequency spectrum for the core SX signals at  $Z = 0.23\text{cm}$  (a), the SX signals at  $Z \approx 12\text{cm}$  (b), and the Mirnov

signals (c). The  $m/n=1/1$  mode in (b) is destabilized nearly simultaneously with the  $m/n=2/1$  mode in (c) whereas the  $m/n=1/1$  mode is measured much later in (a). The vertical solid line labels the moment of the big crash before which the perturbations of the  $m/n=2/2$  mode become stronger as illustrated in (a).

Figure 6. The spatial structures to identify the  $m/n=1/1$  and  $m/n=2/2$  modes. The reconstructions have used the FFT amplitudes and phases of SX signals during the time just before the first big crash.

Figure 7. The reconstructed evolution with FFT amplitudes (a) and with FFT amplitudes and phases (b) for the  $m/n=1/1$  mode. The corresponding results for the  $m/n=2/2$  mode is illustrated in (c) and (d), respectively. It is obvious that the  $m/n=2/2$  mode in (c) grows fast just before the crash indicated by the vertical line, and is located within a much wider space.

Figure 8. (a) The fitted  $q$ -profile according to the value of  $q_{95} = 3.3$  and the assumed centre safety factor  $q_0 = 1.01$ . The vertical bars marked the location of the resultant  $q=2$  rational surfaces. (b) The parametric perturbed flux for the  $m/n=2/1$  mode, the  $m/n=1/1$  mode, and the  $m/n=2/2$  mode. The perturbation at edge is derived from measured perturbed flux before the big crash as illustrated in the figure 4(e). The vertical bar labels the position of  $q=2$ . The relative amplitude and location of  $m/n=1/1$  and  $m/n=2/2$  are determined as shown in figure 7. In addition, the amplitude of  $m/n=1/1$  is supposed to be smaller by the factor  $\varepsilon = a/R_0$  than the

amplitude of  $m/n=2/1$  mode.

Figure 9. The Poincare plots: (a) with the input of the  $m/n=2/1$  mode and the  $m/n=1/1$  mode, (b) with the input of  $m/n=2/1$ ,  $m/n=1/1$ , and  $m/n=2/2$  modes. There is only a little excursion in (a) while the stochastic zones are pronounced for  $r/a < 0.14$  in (b). In particular, there is a braiding as indicated by the arrow, linking the inside stochastic region and the outside nested magnetic surfaces.

Figure 10. The Poincare plots with the same parameters as those in figure 9 except a varying amplitude of  $m/n=2/2$ : (a)  $0.1A_{2,2}$ , (b)  $0.5A_{2,2}$ , (c)  $0.75A_{2,2}$  and (d)  $1.25A_{2,2}$  where  $A_{2,2}$  is the amplitude of  $m/n=2/2$  mode which is used in figure 8(b). The  $\Delta W_n$  labeled by an arrow in (d) indicates the width of a magnetic braiding of  $m/n=2/2$ , which connects the inside stochastic region with the outside nested magnetic surfaces.

Figure 11. The Poincare plots with similar parameters as those in figure 8(b), but a series of  $q_0$ : (a)  $q_0 = 1.01$  the same as the figure 9(b), (b)  $q_0 = 0.99$ , (c)  $q_0 = 0.97$  and (d)  $q_0 = 0.97$  without  $m/n=2/2$  mode. The magnetic braiding in (a) gets narrowed in (b). It is converted into the isolated island of  $m/n=2/2$  in (c) as the  $q_0$  decreases. In addition, the stochastic region gets shrunken with decrease of  $q_0$ . Without the  $m/n=2/2$ , the stochastic region is absolutely absent in (d).

## Figures

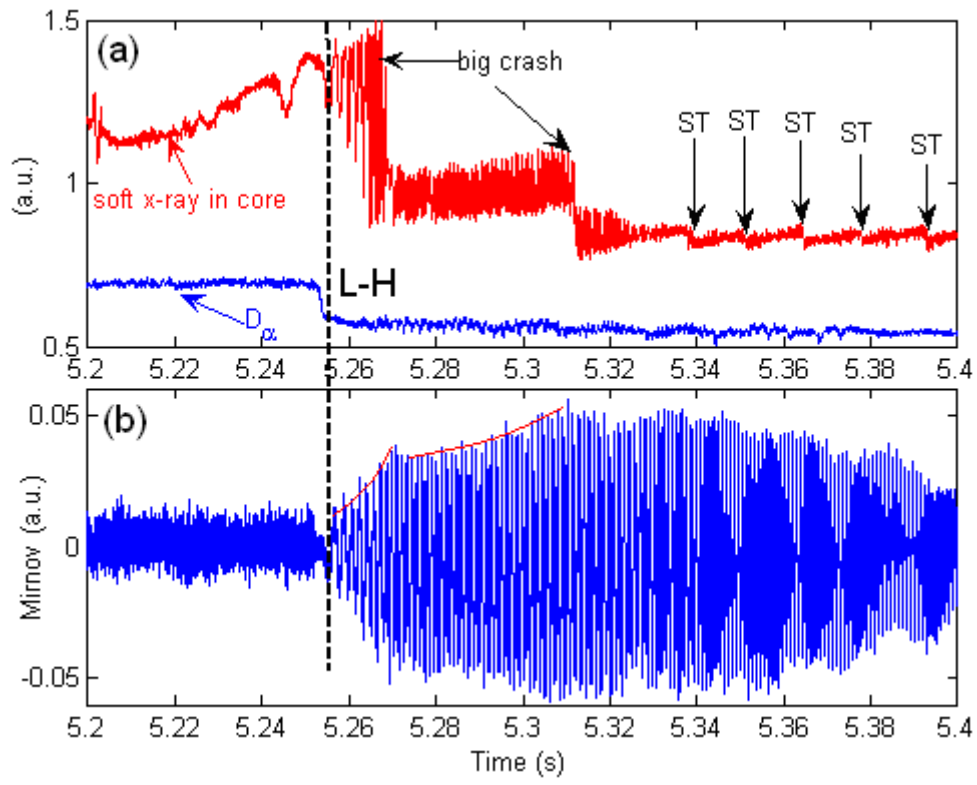


Fig.1

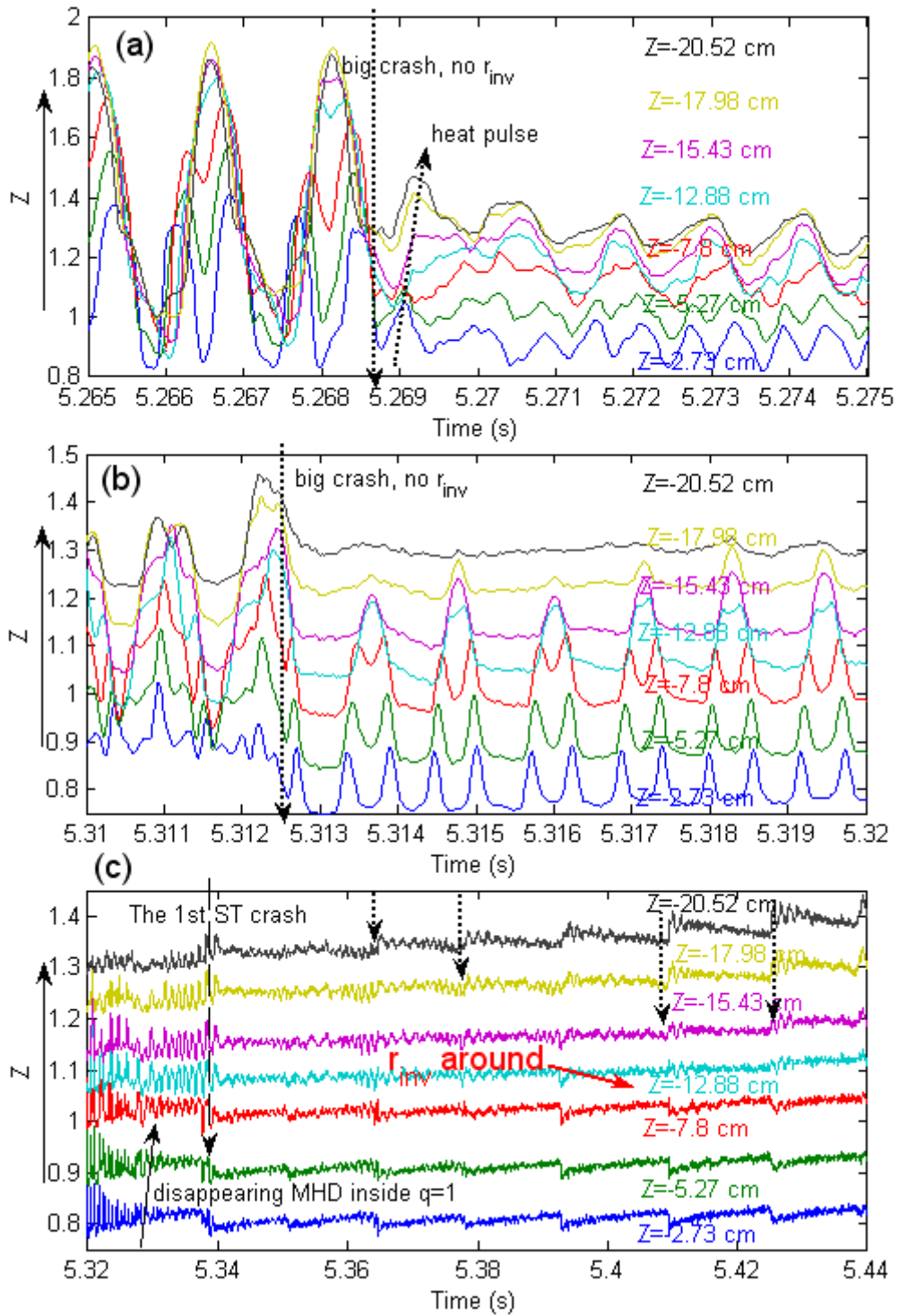


Fig.2

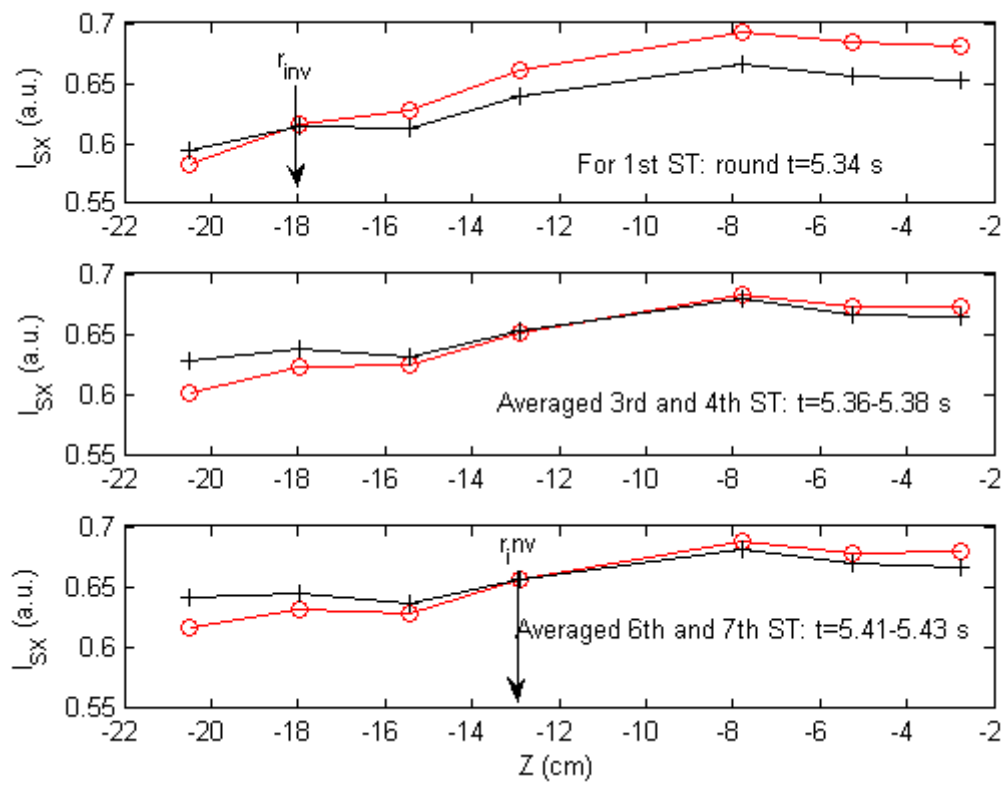


Fig.3

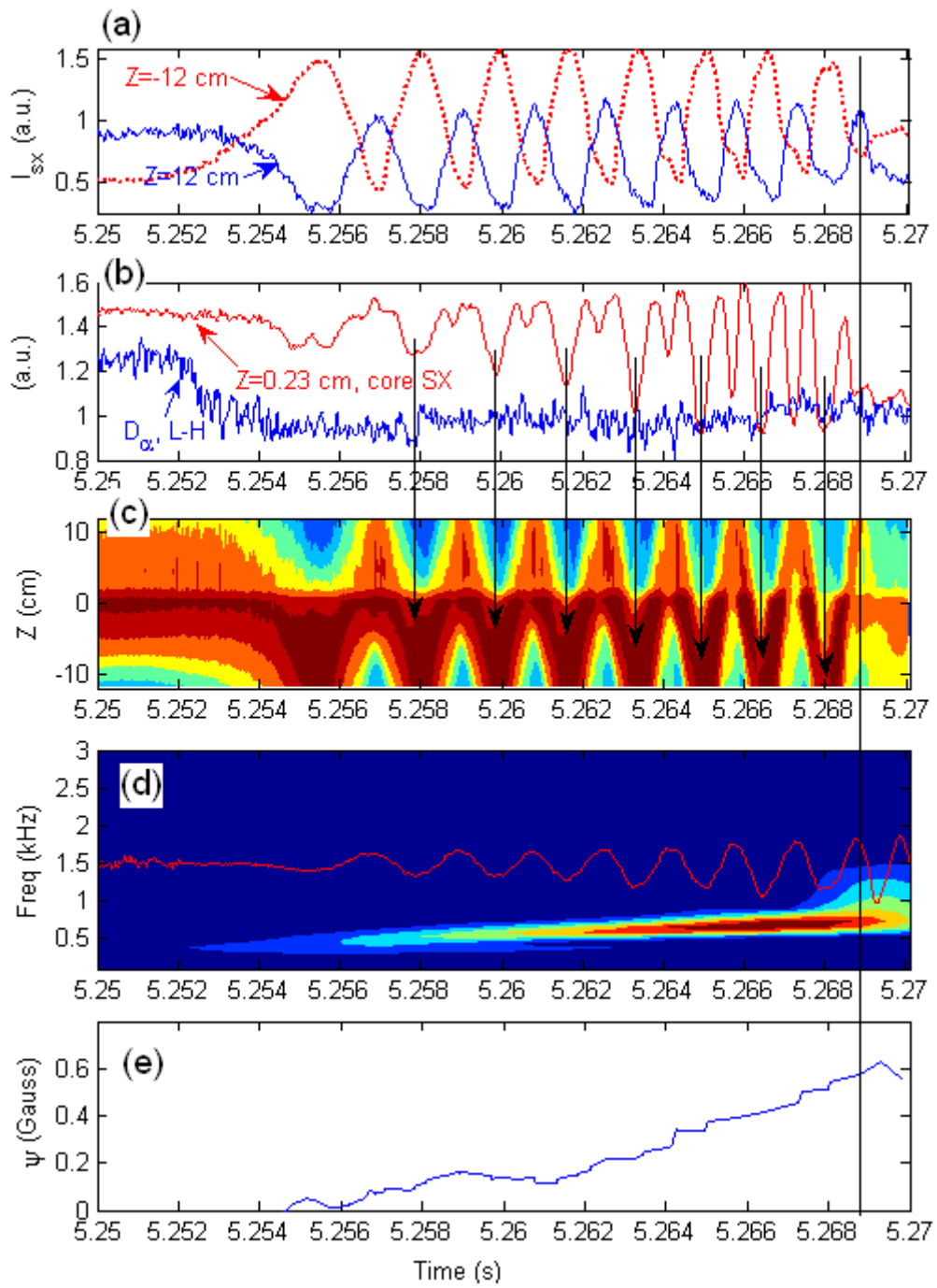


Fig.4



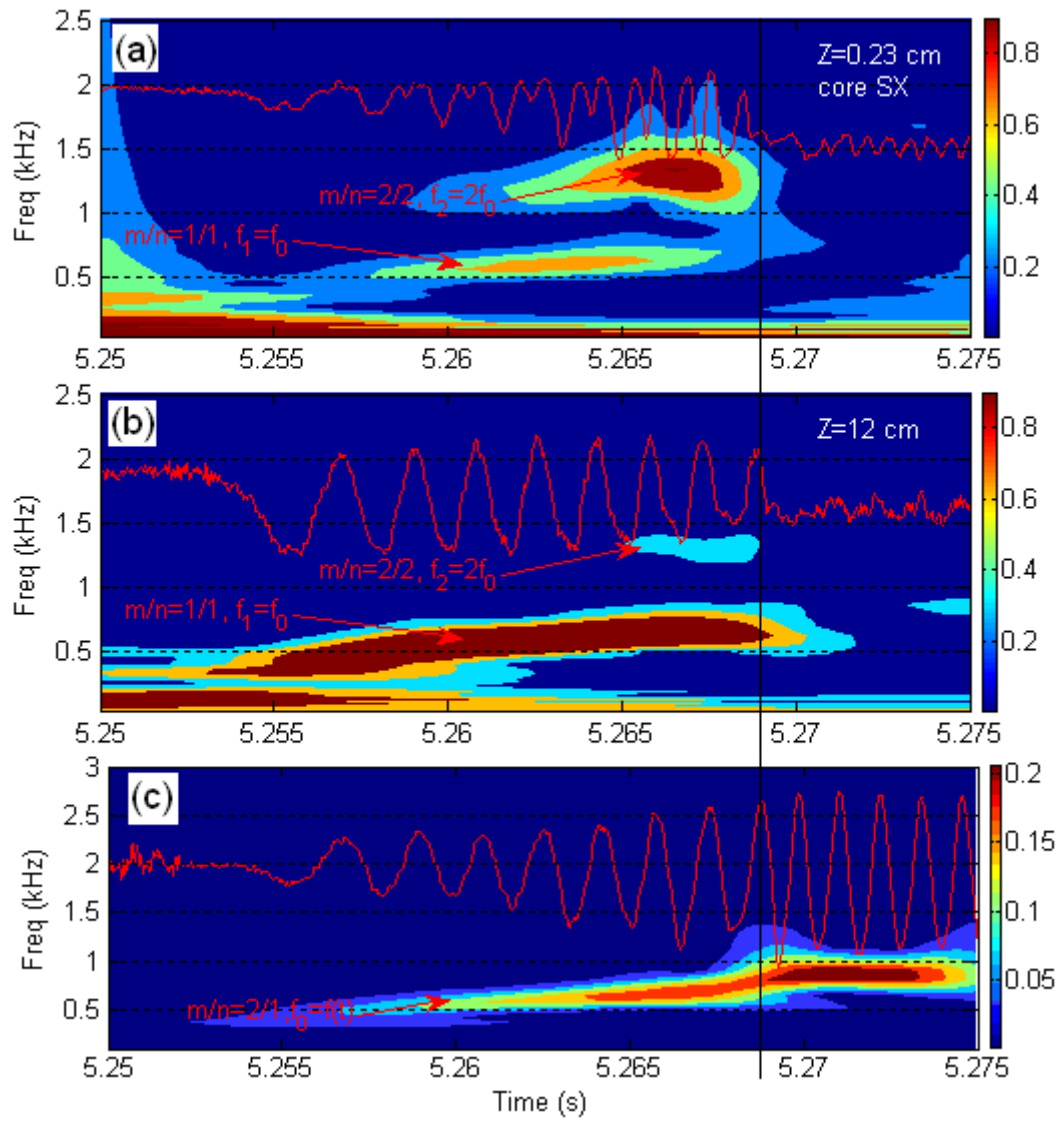


Fig.5

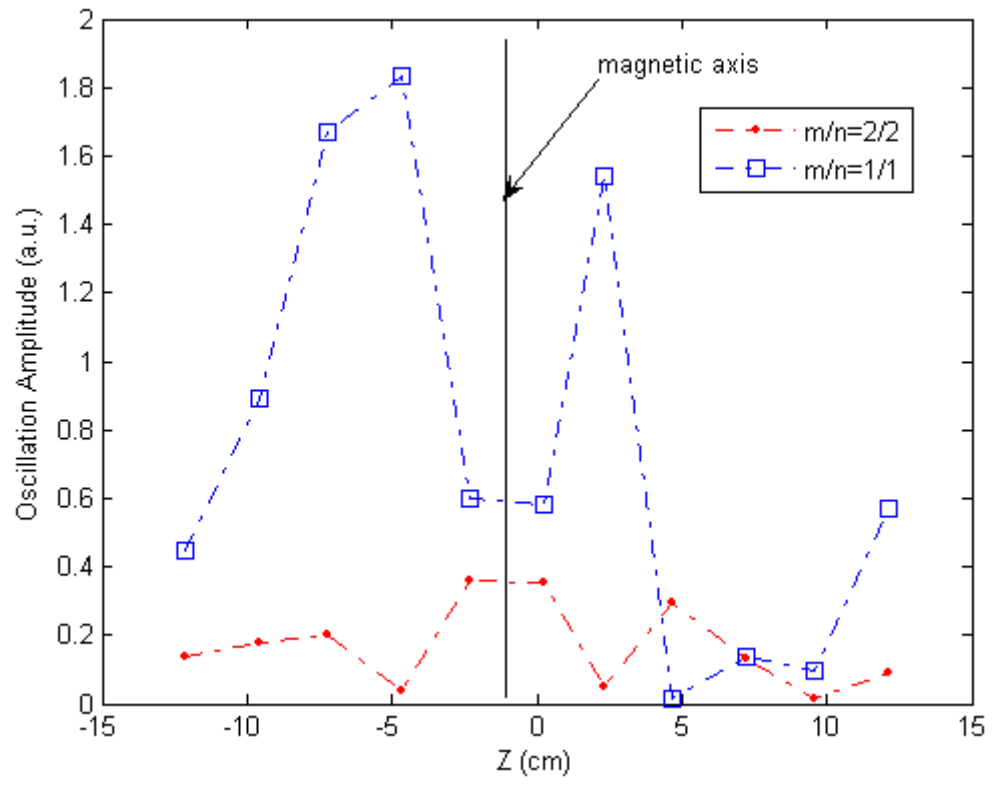


Fig.6

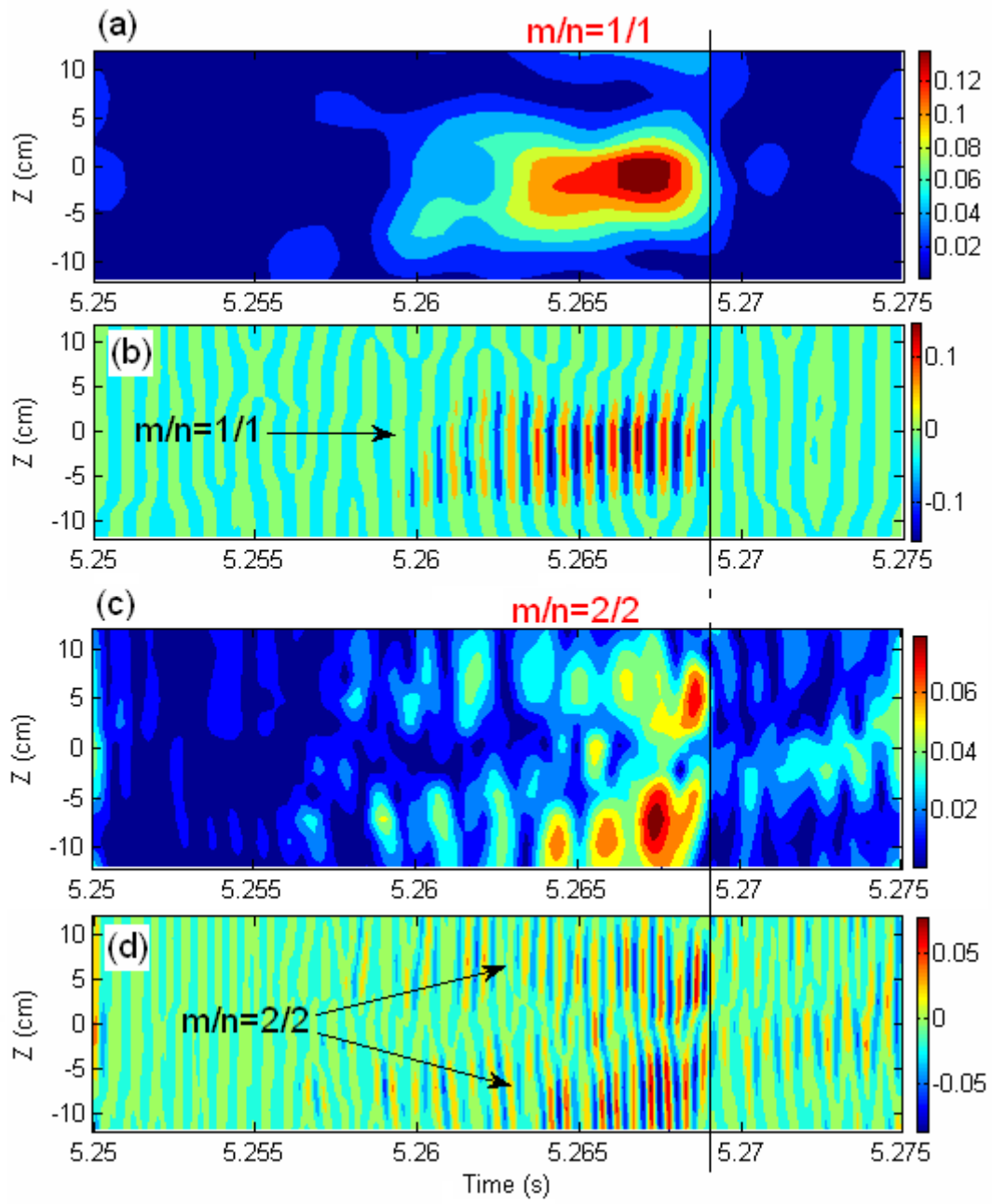


Fig.7

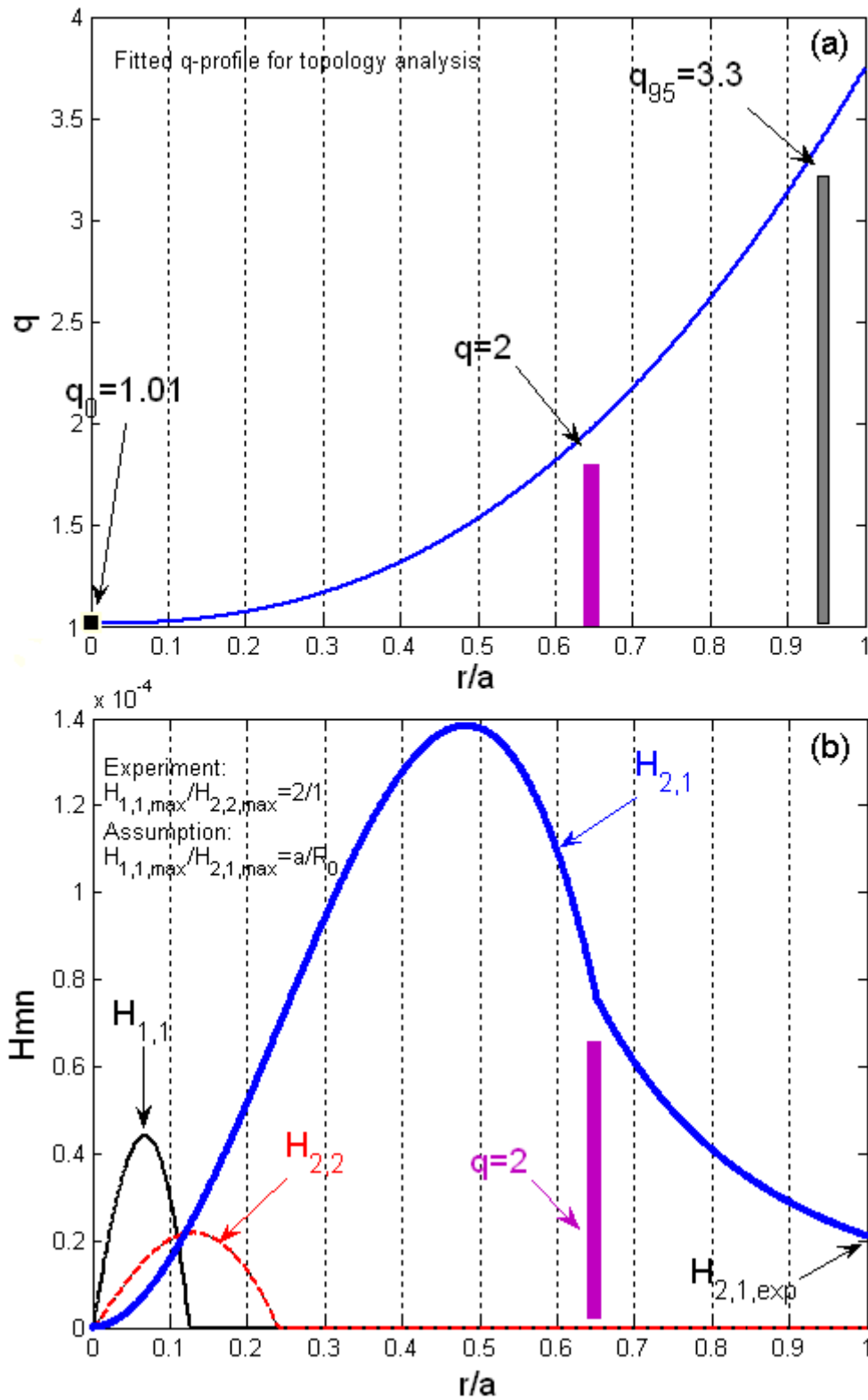


Fig.8

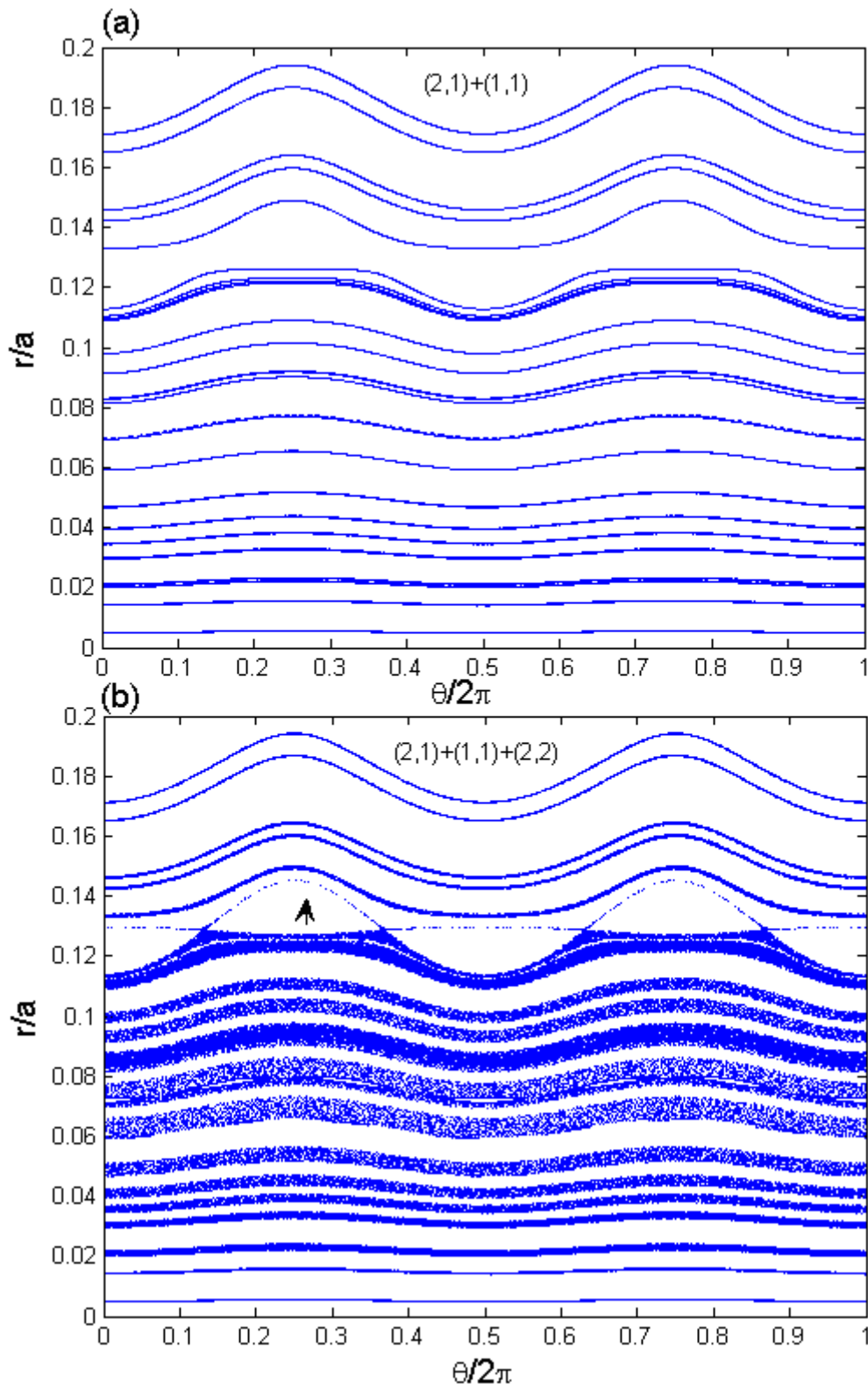


Fig.9

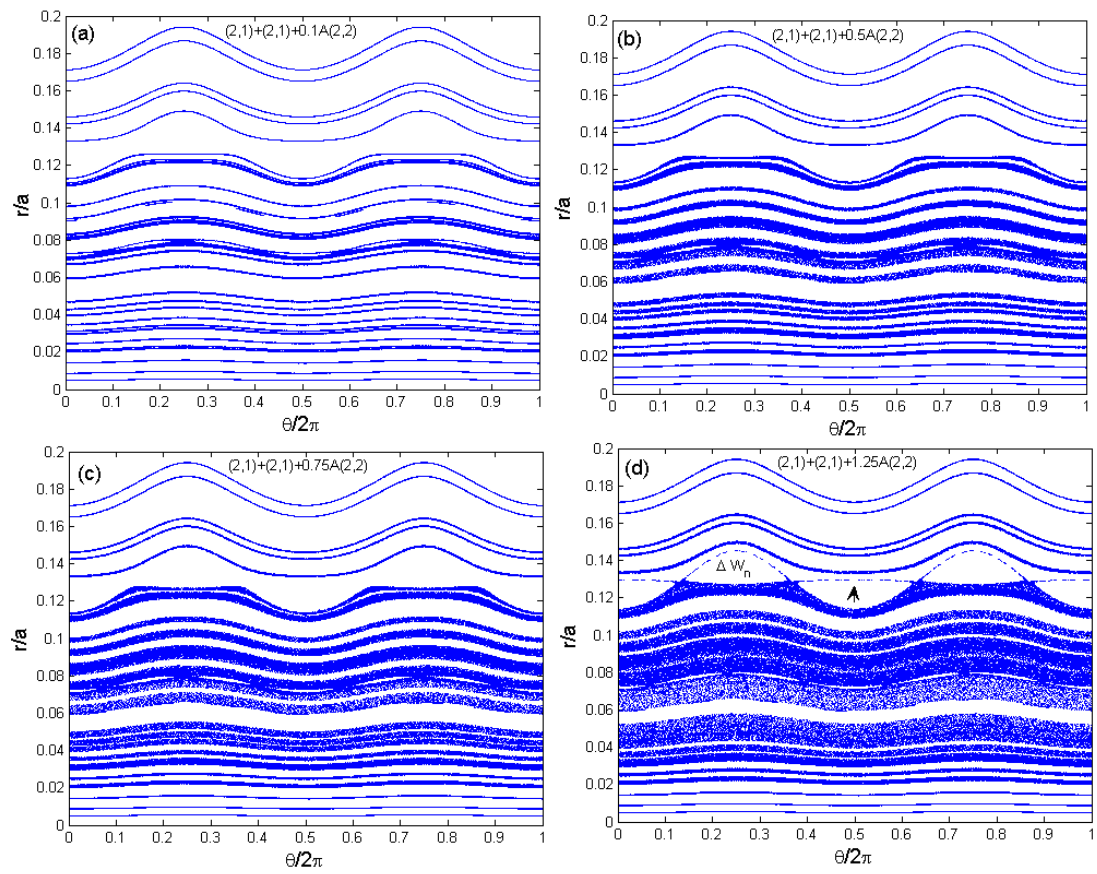


Fig.10

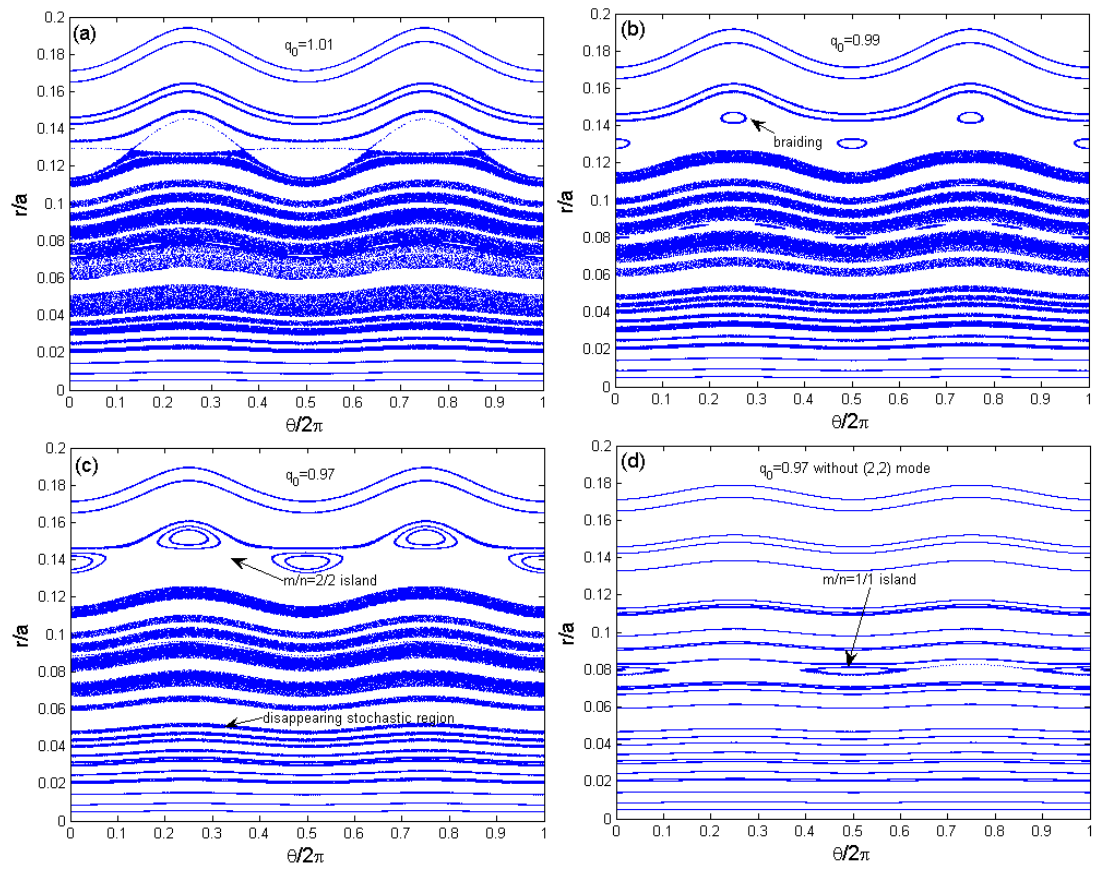


Fig.11